ACS Sustainable Chemistry & Engineering

pubs.acs.org/journal/ascecg

Research Article

Lignin–Chitosan Gel Polymer Electrolytes for Stable Zn Electrodeposition

Naroa Almenara, Robin Gueret, Alberto J. Huertas-Alonso, Unnimaya Thalakkale Veettil, Mika H. Sipponen,* and Erlantz Lizundia*

Cite This: *ACS Sustainable Chem. Eng.* 2023, 11, 2283–2294

Read Online

ACCESS | Metrics & More | Article Recommendations | Supporting Information

ABSTRACT: Electrochemical energy storage technologies offer means to transition toward a decarbonized society and carbon neutrality by 2050. Compared to conventional lithium-ion batteries, aqueous zinc-ion chemistries do not require scarce materials or toxic and flammable organic-based electrolytes to function, making them favorable contenders in the scenario of intensifying climate change and supply chain crisis. However, environmentally benign and bio-based materials are needed to substitute fossil-based battery materials. Accordingly, this work taps into the possibilities of lignin together with chitosan to form gel polymer electrolytes (GPEs) for zinc-ion chemistries. A simple fabrication process enabling free-standing sodium lignosulfonate–chitosan and micellar lignosulfonate–kraft lignin–chitosan GPEs with diameters exceeding 80 mm is developed. The GPEs combine tensile strength with ductility, reaching Young's moduli of 55 ± 4 to 940 ± 63 MPa and elongations at break of 14.1 ± 0.2 to 43.9 ± 21.1%. Competitive ionic conductivities ranging from 3.8 to 18.6 mS cm^{-1} and electrochemical stability windows of up to +2.2 V vs Zn^{2+}/Zn were observed. Given the improved interfacial adhesion of the GPEs with metallic Zn promoted by the anionic groups of the lignosulfonate, a stable cycling of the Zn anode is obtained. As a result, GPEs can operate at 5000 $\mu A\ cm^{-2}$ with no short-circuit and Coulombic efficiencies above 99.7%, outperforming conventional separator–liquid electrolyte configurations such as the glass microfiber separator soaked into 2 M $ZnSO_4$ aqueous electrolyte, which short-circuits after 100 $\mu A\ cm^{-2}$. This work demonstrates the potential of underutilized biorefinery side-streams and marine waste as electrolytes in the battery field, opening new alternatives in the sustainable energy storage landscape beyond LIBs.

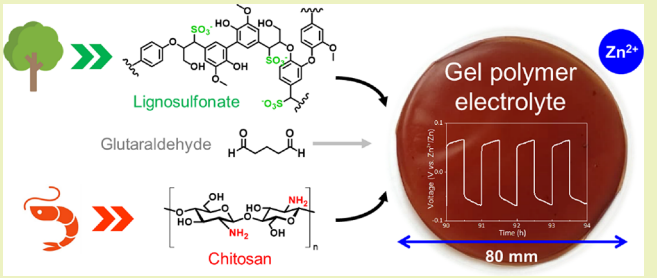

KEYWORDS: *lignin, chitosan, bioeconomy, circular economy, gel polymer electrolyte, zinc-ion battery (ZIB), zinc plating/stripping*

INTRODUCTION

Our society faces serious global challenges associated with the depletion of finite non-renewable resources, environmental pollution, and climate crisis. The current linear economy, following a "take–make–dispose" approach, requires extensive amounts of raw materials that are then processed into goods and once used are finally discarded as a non-biodegradable waste. The extraction and processing of non-renewable materials such as metals or petroleum-based polymers is associated with notable environmental costs, including large carbon dioxide footprints, air and drinking water pollution, biodiversity loss, or eutrophication, among others.[1] Therefore, ambitious initiatives have been set to transition toward a completely circular economy by 2050.[2] In a circular economy, the materials and products are used for as long as possible, which, coupled with lower rates of extraction and exploitation of renewable natural resources, reduces resource depletion and avoids uncontrolled waste accumulation during the end-of-life.[3]

The development of efficient renewable energy conversion and storage technologies is a pressing need to reach sustainable production and consumption patterns that regenerate natural systems.[4,5] The energy transition is pivotal toward climate change mitigation as it may shift from fossil-energy production to renewable-energy sources.[6] Electrochemical energy storage systems are particularly relevant for renewable-energy exploitation given their ability to store and deliver on-demand power.[7] So far, rechargeable lithium ion batteries (LIBs) have been the predominant solution given their relatively high energy-densities, low self-discharge rates, and long operation lifespans.[8] Unfortunately, current LIBs rely on scarce, expensive, and often harmful materials such as lithium, cobalt, manganese, or nickel to function. In addition, flammable organic-based electrolytes are often required, increasing the risk of undesired fires or explosions. As a result, their

Received: September 29, 2022
Revised: January 16, 2023
Published: January 30, 2023

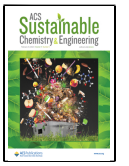

fabrication, use, and end-of-life management poses a number of challenges from an environmental point of view, especially in the long run.[9,10]

Seeking for alternative battery chemistries that offer acceptable electrochemical performance, good safety, and use of earth-abundant and environmentally friendly materials is becoming increasingly urgent. Rechargeable zinc-ion chemistries fulfill these stringent requirements as they rely on zinc ions (Zn^{2+}) as charge carriers.[11] Conventional zinc-ion batteries benefit from the large capacity of Zn (820 mAh g^{-1}).[12] These batteries are composed by a Zn metal negative electrode (anode), a positive electrode (cathode) that enables the reversible Zn^{2+} (de)insertion, and a glass microfiber separator soaked into a liquid electrolyte.[13] Importantly, they do not require dry atmospheric assembly conditions as zinc-ion chemistries could operate with aqueous-based electrolytes, which further enhances their safety and environmental sustainability over LIBs and other multivalent systems (Mg, Ca, and Al).[11] Thereby, aqueous zinc-ion chemistries present significant advantages for stationary energy storage.[14]

The separator−electrolyte pair is a relevant battery component because it determines to a large extent its electrochemical performance (energy density or cycle stability) and safety (thermal stability or resistance against dendrite puncture).[15] This component must ensure adequate ion transference between electrodes at the same time that electronically and physically insulates the anode and the cathode so that internal short circuits and eventual ignition or explosion risks are avoided.[16] The substitution of the porous non-renewable separator soaked into an aqueous electrolyte by a gel polymer electrolyte (GPE) is now pursued by both academia and industry to enhance battery safety by avoiding electrolyte leakage.[17] GPEs typically show an increased compatibility with electrodes given their mechanical flexibility, surpassing liquid electrolyte designs in terms of interfacial compatibility and operating lifetime.[18,19] In addition, GPEs offer increased room-temperature ionic conductivities in comparison with solid-state Zn electrolytes, which usually present conductivities below 10^{-4} mS cm^{-1} due to the high charge density of Zn^{2+}.[20] Usually, GPEs are obtained from petrochemical sources, with polyethylene oxide, polyvinylidene fluoride and its copolymers, or polyacrylonitrile being the most widely found systems.[19] In contrast, if the development of GPEs is accompanied by the use of renewable sources, additional environmental benefits may be obtained. Interestingly, recent works have proven the suitability of biopolymer-derived GPEs to achieve highly reversible and stable metal deposition in batteries.[18,21] Another advantage of many natural polymers is their hydrophilic nature that facilitates ion exchange across the GPE.

As the batteries are becoming common in increasing number of everyday applications, there is a need for large scale biomass resources for GPEs. Underutilized biorefinery wastes offer plenty of materials with abundant functional groups and tailored properties to be exploited as battery electrolytes. So far, most of the efforts to develop Zn^{2+} conducting materials have been directed toward the use of celluloses,[22] agarose,[23] or chitosan.[24] Among the bio-based materials not yet fully exploited, lignin is particularly attractive given its aromatic structure and abundant production as a by-product from industrial biomass processing.[25] Currently, ∼98% of lignin production (from the estimated 80 million ton $year^{-1}$) is combusted for energy recovery purposes, which clearly collides with circular economy principles.[26] This resource waste represents a missed opportunity, particularly when considering recent life cycle assessment (LCA) studies highlighting that when processed into materials and (nano)fillers,[27] lignin can lower the environmental impacts (including CO_2 footprint) over their petro-based counterparts. Therefore, the valorization of lignin into high-value-added products will positively contribute to economics and enhance carbon efficiency of biorefineries.[28] Among lignin-derived materials, sodium lignosulfonate (LS) and kraft lignin (KL), products arising from the sulfite and sulfate pulping process show interesting properties for GPEs. In addition to their phenolic hydroxyl and sulfonic acid groups, the aromatic groups and ether bonds of lignosulfonates can interact with different metal ions through cation−π interactions to enhance ion conduction,[29] yielding GPEs with large ionic conductivities. In addition, the adhesive properties of lignin[30] can be exploited to obtain materials that adhere onto metallic surfaces, enhancing the stability of the electrolyte−electrode interface and enlarging the lifespan of a battery. Sulfonation and subsequent chlorination of pine acid hydrolysis lignin and its combination with poly(vinyl alcohol) has been reported to produce GPEs with an ionic conductivity of 0.25 mS cm^{-1}.[31] However, the potential of sodium lignosulfonate, which is the dominant technical lignin based on today's production quantities, in combination of natural polysaccharides has remained unexplored in GPEs.

Accordingly, here, we report a simple yet effective scalable fabrication of free-standing GPEs consisting of chitosan and lignosulfonate or micellar dispersion of lignosulfonate with softwood kraft lignin, each of the formulations combining renewability, low cost, thermomechanical resistance, ionic conductivity, and electrochemical stability. The gel character of the biopolymer-electrolyte enhances battery safety and environmental sustainability over conventional designs based on microporous fossil-based separators soaked in liquid electrolytes. Importantly, the presence of free water inherent to glass microfibers in the 2 M $ZnSO_4$ aqueous electrolyte system is avoided, suppressing side reactions onto Zn surfaces and thus obtaining longer operation lifespans in symmetric Zn/Zn cells.[32] Obtained results represent a step forward in the development of batteries that use upcycled biorefinery waste streams.

EXPERIMENTAL SECTION

Materials. Softwood kraft lignin (KL, BioPiva 100 pine kraft lignin (UPM, Finland), lignosulfonate (LS, DS10, Domsjö, Sweden). Chitosan (50,000−190,000 Da), glutaraldehyde (50 wt % in H_2O), and zinc sulfate monohydrate ($ZnSO_4{\cdot}H_2O$) have been purchased from Sigma-Aldrich. The carbon paper (TP-060-T5) was purchased from QuinTech. Electrolytes were prepared using ultrapure water (18.2 MΩ cm). All chemicals were used as received without any further purification. For electrochemical studies, glass microfiber separators (GF/A, Whatman) were employed as received. Zn foil (0.25 mm thickness) was obtained from Thermo Fisher Scientific.

Fabrication of Gel Polymer Electrolytes. As summarized in Figure 1, lignosulfonate−chitosan gel polymer electrolytes were synthesized using LS or a micellar dispersion of lignosulfonate−kraft lignin (LSKL).[33] Four samples of two different compositions of LSKL−chitosan and LS−chitosan were prepared, obtaining a lignin content of 10 and 30 wt % in the final membrane. Chitosan was added to a minimum of 70 wt % to improve the film-forming ability while ensuring adequate electrochemical properties (lower chitosan concentrations fail to form free-standing membranes). Table S1 in the Supporting Informationgives additional details on each sample

https://doi.org/10.1021/acssuschemeng.2c05835
ACS Sustainable Chem. Eng. 2023, 11, 2283−2294

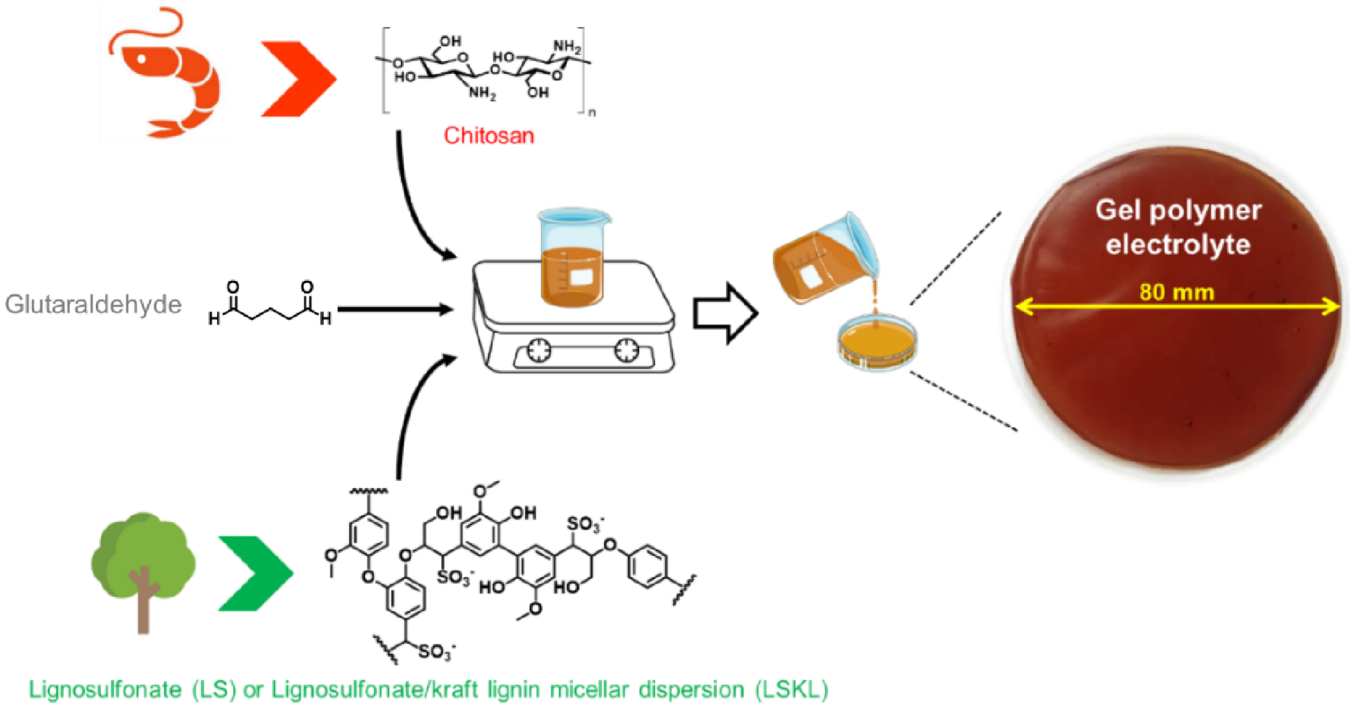

Figure 1. Schematic representation of the fabrication process of LS−chitosan and LSKL−chitosan gel polymer electrolytes.

composition along with the nomenclature. Glutaraldehyde was used as a chemical cross-linker to enhance the physical integrity of the gels.

Preparation of Lignosulfonate−Kraft Lignin−Chitosan Membranes. The chitosan solution (1 wt % in 1 wt % of acetic acid) was added to a vial containing a predetermined amount of KL-LS gel dispersion (43 wt %). The mixture was stirred for 3 days until homogenization was attained. Then, for the cross-linked samples, 50 wt % glutaraldehyde was added to the homogenized solution and the mixture was stirred at 500 rpm for 30 min. After that, the samples were casted on polypropylene Petri dishes (⌀ = 80 mm) and allowed to cross-link for 3 days at room temperature in the fume hood. GPEs of 250 ± 70 μm thickness were obtained after immersing the films into a 2 M $ZnSO_4$ aqueous solution overnight.

Preparation of the Lignosulfonate−Chitosan Samples. Lignosulfonate solution (1 wt %) was dropwise added to a chitosan 1 wt % solution in 1 wt % of acetic acid under magnetic stirring using a syringe pump at a flow rate of 15 mL h^{-1}. The mixture was stirred for 3 days until homogenization was attained. Then, for the cross-linked samples, 50 wt % glutaraldehyde was added to the homogenized solution and the mixture was stirred at 500 rpm for 30 min. After that, the samples were casted on polypropylene Petri dishes (⌀ = 80 mm) and allowed to cross-link for 3 days at room temperature. GPEs of 250 ± 70 μm thickness were obtained after immersing the films into a 2 M $ZnSO_4$ aqueous solution overnight.

Membrane Characterization. Field-emission scanning electron microscopy (FE-SEM) analyses were carried out using a Hitachi S-4800 at an acceleration voltage of 5 kV. Before the morphological observations of the cryo-fractured surfaces, the samples were sputtered with a 10 nm-thin gold−palladium layer. Powder X-ray diffraction (XRD) patterns were obtained with a D8 Discover diffractometer in reflection mode using Cu Kα radiation (45 kV, 40 mA). Attenuated total reflectance Fourier transform infrared (ATR-FTIR) spectroscopy results were obtained using a Varian 610-IR FT-IR spectrometer equipped with diamond ATR optics.

The thermal degradation behavior of gel electrolytes was studied by means of thermal gravimetric analysis (The Discovery TGA) in platinum oxide pans under air atmosphere at a heating rate of 10 °C min^{-1} and 50 mL min^{-1} for each sample (2 to 7 mg). The mechanical behavior of samples was studied by uniaxial tensile tests using a universal testing machine (Trapezium Shimadzu AGS-X) equipped with a 100 N load cell at a deformation rate of 1 mmmin^{-1}. Specimens 20 mm long and 6 mm wide with thicknesses of 250 ± 70 μm were used. The mean average value and standard deviation Young's modulus (E) (from 0.5−1% strain region), stress and strain at yield (σ_y and ε_y, respectively), and stress and strain at break (σ_b and ε_b, respectively) were determined from four measurements.

The electrolyte uptake (EU) of lignin gel electrolytes was measured after immersion of the LSKL−chitosan and LS−chitosan membranes in 0.5, 1, and 2 M $ZnSO_4$ aqueous solution for 24 h as

$$\mathrm{EU} = \frac{100}{m_{\mathrm{dry}}} \times (m_{\mathrm{wet}} - m_{\mathrm{dry}}) \quad (1)$$

where m_{wet} and m_{dry} are the weight of the wet and dry lignin gels, respectively.

Electrochemical studies were carried out using a VMP3 Biologic electrochemical workstation. Gel electrolytes (diameter = 13 mm; area = 1.327 cm^2) were assembled into Swagelok-type cells at room temperature. For ionic conductivity measurements, gel electrolytes were sandwiched between two stainless steel rods. Electrolyte resistance was measured using a two probe AC impedance spectroscopy analyzer with a 5 mV voltage amplitude in the frequency range from 1 Hz to 5 MHz. The resistance was measured from the high-frequency intercept on the real axis in the Nyquist plots, and the ionic conductivity (σ_i) was obtained according to

$$\sigma_i = \frac{d}{R_b \times A} \quad (2)$$

where d is the gel thickness, R_b represents the bulk resistance extracted from the intercept of the curve with the real impedance axis in the Nyquist plot, and A accounts for the contact area of the gel electrolyte and the stainless steel rod.

In addition, the electrochemical stability window was studied by voltammetric measurements, where gel electrolytes were sandwiched between a carbon paper as the working electrode and a Zn metal disk as the reference and counter electrode. The voltammograms were obtained in the potential range of −0.25 V to +2.4 V vs Zn^{2+}/Zn with a scan rate of 1 mV s^{-1} using a VMP3 Biologic instrument.

Zn stripping and plating performance was studied under different current densities from ±50 to ±500 μA· m^{-2}. To that end,

https://doi.org/10.1021/acssuschemeng.2c05835
ACS Sustainable Chem. Eng. 2023, 11, 2283−2294

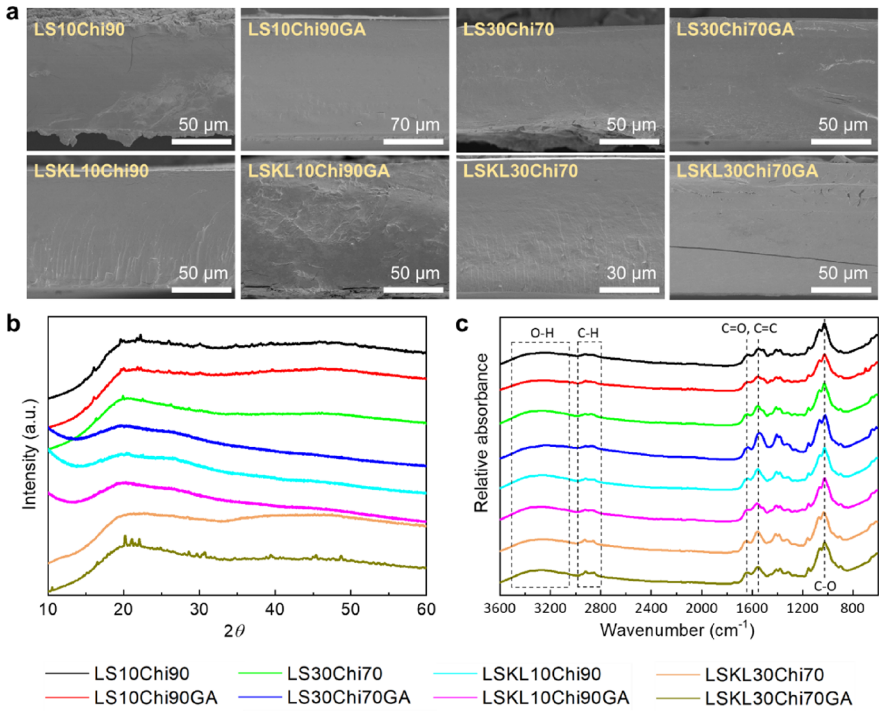

Figure 2. (a) Representative SEM micrographs showing the cross sections of the GPEs with varied compositions. (b) XRD patterns and (c) ATR-FTIR spectra of synthesized GPEs. The scale bar size for SEM images varies due to the slight differences in film thickness.

lignosulfonate−chitosan and LSKL−chitosan GPEs were mounted between two Zn-metal discs. For the sake of comparison, Zn stripping and plating was also performed using a glass fiber separator soaked in a 2 M $ZnSO_4$ aqueous solution. For post-mortem SEM studies, the cycled Zn surfaces were washed with water before drying under vacuum.

RESULTS AND DISCUSSION

Morphological and Structural Characterization. A scalable fabrication process for GPEs is developed using underutilized biorefinery wastes as a source material while enabling a rapid and stable Zn^{2+} transport. Our efforts have been focused on the use of lignosulfonate and chitosan as the polymeric constituents for free-standing membrane formation, which after immersion in 2 M $ZnSO_4$ H_2O yield ionically conducting GPEs. Preliminary experiments showed the inability to achieve lignin-only GPEs due to their poor film-forming properties. In this sense, chitosan was incorporated at 70 and 90 wt % as a model polysaccharide to improve the film-forming ability.[34] The morphology of the resulting GPEs after freeze-drying was investigated by scanning electron microscopy (SEM), and the cryo-fractured cross sections are shown in Figure 2a. The obtained dense and smooth structure with no voids or crystalline aggregates observed for all the compositions indicates the uniform dissociation of the zinc salt within the polymeric gel. This feature is particularly interesting as it is considered a prime requisite to achieve a homogeneous ion transport across the GPE and offer a stable ion electrodeposition onto Zn. An increased amount of lignin yields brownish GPEs (Figure S1). As shown in Figures S2 and S3, the developed approach is simple and scalable enough to result in homogeneous, free-standing, and mechanically flexible GPEs with diameters above 80 mm.

Amorphous electrolytes are preferred as the crystalline regions generally present an increased resistance for the transport of ions.[35] Lignins are known to be amorphous, but chitin, the precursor of chitosan, can form crystalline domains.[36] Accordingly, the occurrence of crystalline phases has been assessed by X-ray diffraction experiments. As shown in Figure 2b, all the GPEs present an amorphous halo with a broad peak centered at $2\theta = 20.5°$ originating from the overlap of the (110) crystal plane of chitosan ($2\theta = \sim 19.2°$),[37] together with the broad band at $2\theta = 22°$ of stacked lignin aromatic layers into the (002) plane (see the diffraction patterns of the biopolymer GPE components in Figure S4).[38] As opposed to bare $ZnSO_4$ salt, which forms a crystalline structure with well-differentiated and narrow diffraction peaks (Figure S4),[39] the GPEs here synthesized present low intensity sharp peaks, indicating the coexistence of large amorphous regions with few crystalline phases. Overall, the predominant amorphous halo for all the GPEs suggests the ability of lignin−chitosan blends for complexation and dissolution of $ZnSO_4$, enabling a low barrier for ion diffusion for the migration of Zn^{2+} through these amorphous phases (note, on the contrary, the highly crystalline character of the $ZnSO^4$ salt in Figure S4).[40] Attenuated total reflectance−Fourier transform infrared (ATR-FTIR) spectra in Figure 2c present the characteristic absorption bands of lignin, with a band at 1000 cm^{-1} assigned to C−O deformation and aromatic C−H in plane deformation, 1550 and 1650 cm^{-1} (aromatic skeletal vibrations and C═O stretch), 2800−3000 cm^{-1} C−H stretch in methyl groups in LS and methylene groups of LS and chitosan, and a broad band at 3100−3500 cm^{-1} assigned to hydroxyl groups in chitosan and lignin.[41]

Thermal and Mechanical Properties. The development of GPEs with acceptable thermal stabilities is an essential prerequisite toward battery safety so that the likelihood of thermal runaway is reduced. Thermogravimetric analysis (TGA) is commonly used to assess the thermal stability of battery separators. The TGA curves under air atmosphere

https://doi.org/10.1021/acssuschemeng.2c05835
ACS Sustainable Chem. Eng. 2023, 11, 2283−2294

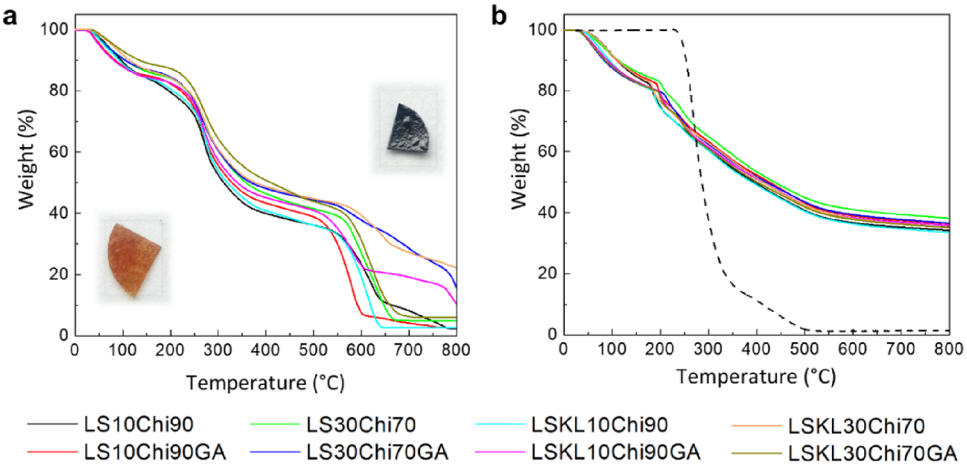

Figure 3. TGA traces under air atmosphere for (a) LS−chitosan and LSKL−chitosan membranes and (b) corresponding GPEs. Dashed line: Celgard 2325 membrane. The insets in (a) show the LS10Chi90 sample before and after TGA measurement.

shown in Figure 3a for LSKL−chitosan and LS−chitosan membranes (before $ZnSO_4$ soaking and no Zn salts) show an initial weight loss of 10−15 wt % at 75 °C, resulting from the adsorbed moisture evaporation. A marked thermodegradation event occurs in the temperature range of 245−400 °C. This weight loss arises from pyrolysis of the biopolymer involving fragmentation of the inter-unit linkages between phenolic and carbonyl groups and the release of monomeric phenols in lignin[30] as well as the deacetylation and cleavage of glycosidic linkages in chitosan.[42] Finally, a decomposition of the residual carbon occurs. In addition, Figure 3b shows the thermodegradation traces for the GPEs, which are obtained after soaking the membranes into 2 M $ZnSO_4$ H_2O. The mass loss event at nearly 200 °C arises from the water loss resulting from $ZnSO_4$ salt crystallization.[43] Interestingly, $ZnSO_4$ exerts a retarding effect on mass loss for all the studied formulations, particularly during the second and third degradation stages at temperatures above ∼300 °C. In particular, the GPEs reach their 50% weight loss at 390−438 °C (depending on the composition) in comparison with the 311−408 °C observed for the membranes without the electrolyte. For the sake of comparison, as highlighted by the dashed line, the microporous polyolefin Celgard 2325 separator (composed by petro-based polypropylene and polyethylene) reaches the 50% weight loss at 284 °C.[44] This flame retardancy effect of lignin is consistent with previous studies, which ascribed such behavior due to the formation of intumescent char layers efficiently limiting the heat and flammable volatile transfer.[43,45] In addition, the marked increase in the residual mass at 700 °C from 2.5 wt % for KL-LS/Chi 10/90 to 36 wt % for its GPE counterpart is explained by the effective flame retardant role of zinc sulfate by promoting the formation of charring layers. A similar effect was also found in polypropylene-based composites.[45] The amount of char residue slightly increases with lignin amount (either KL or LS) given the tendency of aromatic rings to yield carbonaceous structures. The improved thermal stability after impregnation with $ZnSO_4$ together with the larger char residue at high temperatures indicates that LSKL−chitosan and LS−chitosan GPEs are appealing to physically isolate battery electrodes (anode and cathode) at high temperatures, avoiding the risk for short-circuit upon thermal runwaway.[46]

Mechanical properties of GPEs should be also considered when designing safe batteries with long-operation life spans. In particular, mechanically adaptable and ductile electrolytes typically show an enhanced interfacial contact with metallic electrodes, while stiff GPEs offer a physical barrier against undesired dendrite growth.[47] Uniaxial tensile stress−strain experiments were conducted to evaluate the Young's modulus (E), tensile stress at yield and at break (σ_y and σ_b), and elongation at yield and at break (ε_y and ε_b). Representative stress−strain curves can be seen in Figure 4a, while Table S2 summarizes the main characteristic parameters. The glass microfiber separator presents a stiff and brittle character, with a modulus of 1470 ± 120 MPa and ε_b of ∼5.8 ± 0.1%.[48] On the contrary, as schematized in Figure 4b, LSKL−chitosan and LS−chitosan GPEs show a semi-ductile behavior characterized by E values ranging from 55 ± 4 to 940 ± 63 MPa and ε_b values of 14.1 ± 0.2 to 43.9 ± 21.1% (Figure 4c,d). For the sake of comparison, the most widely exploited GPE, the polyethylene oxide/LiTFSI blend, displays a Young's modulus of ∼100 MPa.[15] Independently of the composition, we found that glutaraldehyde cross-linking increases stiffness and lowers ductility due to the formation of extended imine linkages in the electrolyte. An increased fraction of lignin lowers both E and ε_b values as reported for chitosan-lignin films,[49,50] while the micellar LSKL dispersion results in stiffer but more brittle GPEs in comparison with LS−chitosan GEPs.[51] Overall, the GPEs here developed show an enlarged ductility while keeping acceptable tensile modulus values, offering an advantageous resistance against dendrite penetration.[52] The mechanical flexibility of the GPEs also facilitates battery cell assembly while ensuring a good interfacial contact with metallic Zn due to the ability to accommodate electrode volume changes upon Zn^{2+} insertion/extraction.[53]

Electrochemical Characterization. The predominantly amorphous character of the GPEs together with the abundant hydroxyl functional groups (4.12 mmol g^{-1})[33] available to interact with Zn^{2+} of the GPEs encourage their use as ionic conductors for batteries. The electrolyte uptake was quantified based on eq 1 after soaking the membranes into 0.5, 1, and 2 M $ZnSO_4$ H_2O for 24 h. EU values ranging from 78 to 319 wt % were obtained for various membrane compositions (Figure 5a). No marked changes depending on KL or LS are achieved. Glutaraldehyde cross-linking lowers electrolyte uptake values as the amount of groups to interact with water are reduced.[54] An increase in the lignin content (at expenses of a decrease of

https://doi.org/10.1021/acssuschemeng.2c05835
ACS Sustainable Chem. Eng. 2023, 11, 2283−2294

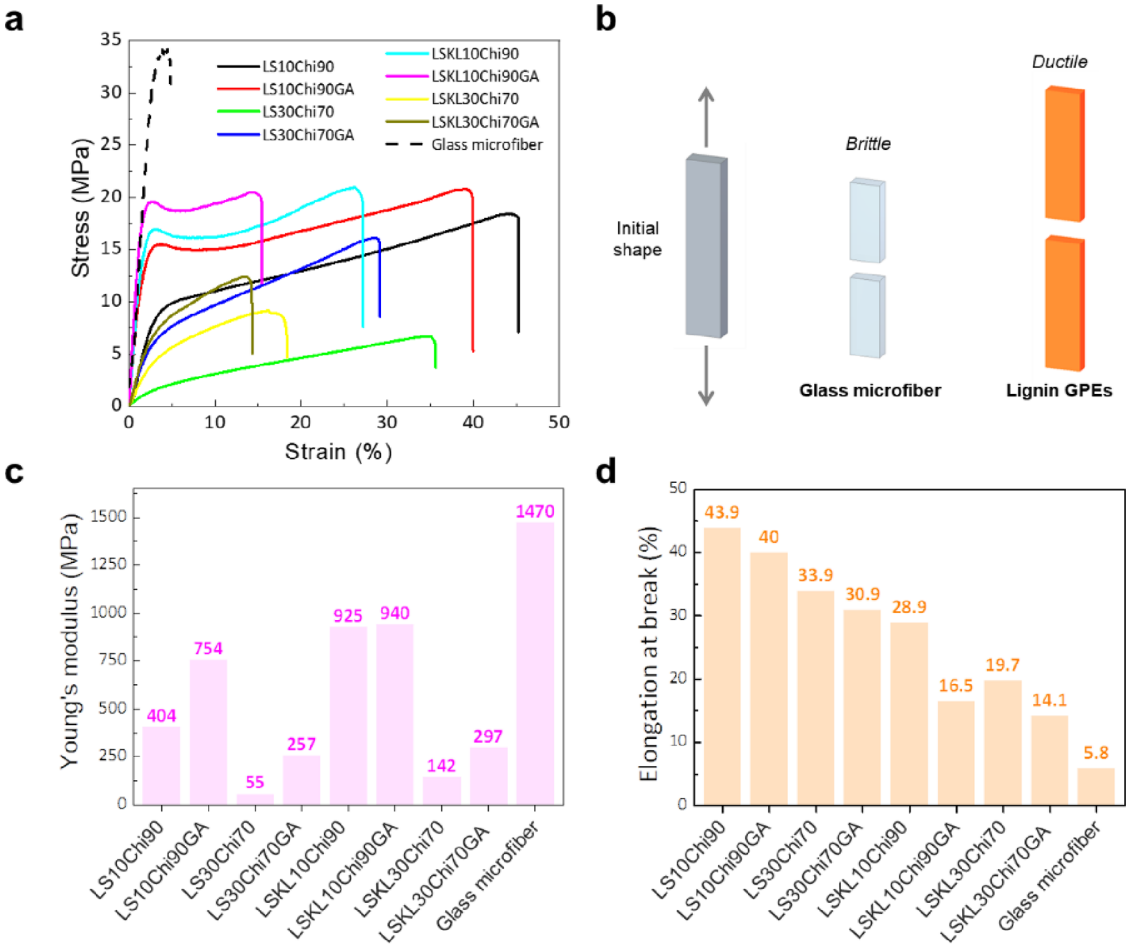

Figure 4. Mechanical characterization with (a) representative stress−strain curves together with (b) a schematic illustration showing the mechanical characteristics of glass microfiber separator and lignin GPEs. Mean values of (c) Young's modulus and (d) elongation at break of LS−chitosan and LSKL−chitosan GPEs. Data corresponding to glass microfiber is shown for comparison.

chitosan) also results in a lowered electrolyte uptake despite the phenolic hydroxyl groups and carbonyl groups being active water sorption sites in lignin.[55] Though KL and LS are not hydrophobic materials as such, the presence of hydrophobic rings as opposed to the abundant polar groups of chitosan lends explanation to the lower electrolyte uptake in the presence of lignin.[56] It is also observed that larger electrolyte uptake values are achieved when increasing $ZnSO_4$ concentration. It is important to note that measured water uptake values are larger than the ∼14−16 wt % shown for organosolv/Nafion/polyethylene oxide or organosolv/Nafion membranes[57] or the 28.5−34.5 wt % obtained for sulfonated poly(ether ether ketone)/lignin membranes[58] and comparable to the 230 wt % shown by lignin membranes impregnated in solutions of organic carbonates.[59] These results indicate the suitability of Kraft lignin−chitosan and lignosulfonate−chitosan to provide efficient medium for Zn^{2+} transport.

Zn^{2+} conductivity values have been obtained from the Nyquist impedance plots in Figure S5 using the eq 2 (further details are provided in Tables S3−S5). All the GPEs display straight lines with no semicircles as a result of their ionically conducting character. As summarized in Figure 5b, ionic conductivities from 3.8 to 18.6 mS cm^{-1} are achieved for the GPEs. Larger values of 15.0 and 59.3 mS cm^{-1} are observed for the glass microfiber separator soaked in 0.5 and 2 M $ZnSO_4$ H_2O, respectively. However, lignin−GPE conductivities are superior to the 0.12 mS cm^{-1} reported for a carboxymethyl cellulose/$ZnSO_4$ GPE,[60] * the 14.6 mS cm^{-1} shown for xanthan gum/$ZnSO_4$/$MnSO_4$ GPE,[61] or the 8.9 mS cm^{-1} of chitosan/choline nitrate GPEs.[62] We also achieved larger values compared to the reported lignin-derived GPEs intended for LIBs, including 3.73 mS cm^{-1} showed by a GPE obtained upon soaking lignin fibers into 1 M $LiPF_6$ ethylene carbonate/dimethyl carbonate/ethyl methyl carbonate[59] or 2.52 mS cm^{-1} obtained for a polyvinylpyrrolidone/lignin soaked into the same system as above.[63] Similarly, obtained conductivities are above the numbers reported for porous membranes soaked in zinc salt aqueous solution, such as the 9.1 mS cm^{-1} obtained for a Nafion/lignin membrane soaked into 2 M $ZnSO_4$ H_2O.[64] A plausible explanation may be the coordination of Zn^{2+} mobile charge species with the hydroxyl groups in chitosan and lignin as well as carboxylic and sulfonate groups of lignin, together with the lone pair on the N atom and O atom in chitosan coordinating with Zn ions and the phenol hydroxyl groups of lignin that dissociate the anion from the salt,[59] facilitating Zn^{2+} movement. In addition, the 3D structure of LS, having vast sulfonate, polar ether, and hydroxyl groups forms ionic domains with highly mobile water molecules,[54] further boosting Zn^{2+} conductivity. These characteristics enable obtaining GPEs with a good compromise between mechanical properties (stiff but ductile) and ionic conductiv-

https://doi.org/10.1021/acssuschemeng.2c05835
ACS Sustainable Chem. Eng. 2023, 11, 2283−2294

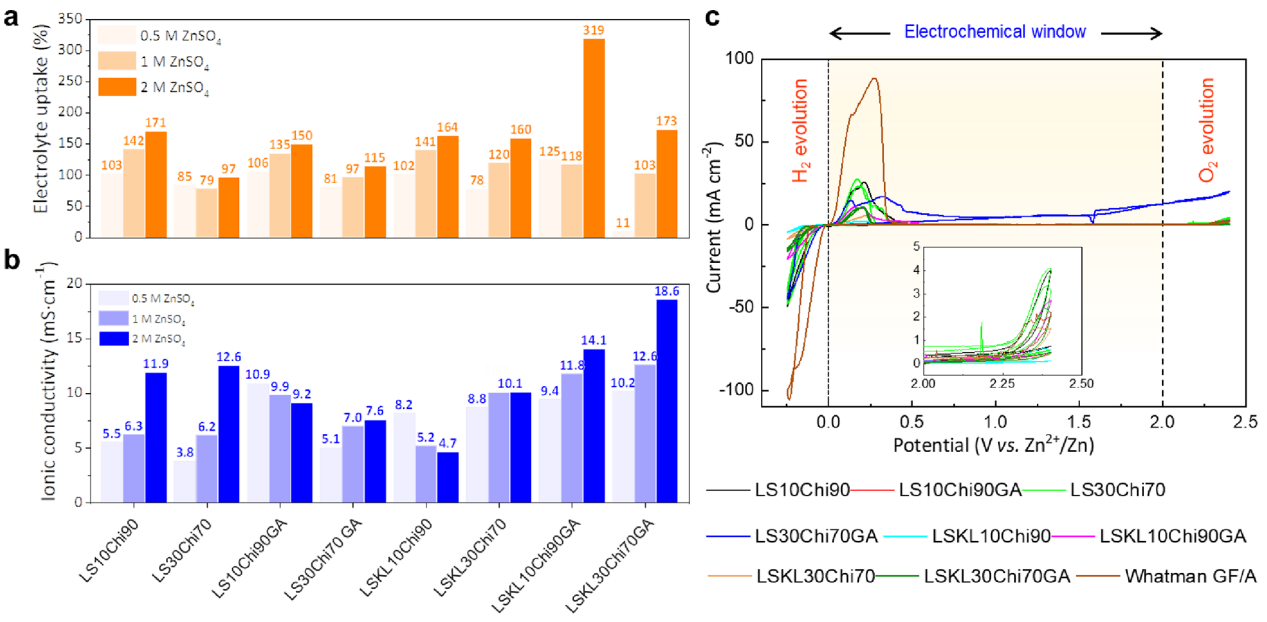

Figure 5. (a) Electrolyte uptake; (b) ionic conductivity and (c) electrochemical stability window LS−chitosan and LSKL−chitosan GPEs. The inset shows an expanded view of the oxygen evolution reaction region.

ities in the mS cm^{-1} order, often conflicting requirements in the polymer electrolyte field.[65,66]

Aqueous Zn cell failure is usually triggered by hydrogen evolution reactions and corrosion reactions of the metallic Zn anode, limiting the practical ability of zinc-ion batteries.[67] As the extent of the initial overpotential obtained for Zn plating on a smooth Zn foil is related to the hydrogen produced, the electrochemical stability window of GPEs in the potential range of −0.25 to +2.4 V vs Zn^{2+}/Zn has been assessed. As indicated by the low current peaks in Figure 5c, the overall stability window expands up to +2.2 V vs Zn^{2+}/Zn with hydrogen and oxygen evolution reaction potentials enlarged in comparison to the glass microfiber separator soaked in the liquid electrolyte. Particularly, the onset overpotential for hydrogen evolution reaction is notably shifted cathodically by 20−50 mV for all GPEs. As a result, the system here explored can be useful with high-voltage cathodes such as cobalt hexacyanoferrate.[11] This observation matching previous reports that highlight the wide electrochemical stability of lignin in LIBs[59,68] is ascribed to the adhesion of the GPE to the electrode surface to provide a passivation layer.[11] Importantly, lignosulfonate−Kraft lignin−chitosan and lignosulfonate−chitosan GPEs present a 4.5- to 18-fold reduction on the anodic and cathodic intensity peaks at ∼0 V in comparison with the glass microfiber separator soaked into 2 M $ZnSO_4$ H_2O as a result of the hydrogen evolution reaction depletion by lignin GPEs.[67] The reduced resistance to Zn anodic dissolution and Zn cathodic deposition process provided by the biopolymer GPEs is further confirmed by Zn/Zn symmetrical cell results.

The electrochemical performance of the GPEs has been further investigated using a symmetric Zn/Zn cell configuration at room temperature. Importantly, this technique provides information regarding the reversibility of the Zn^{2+} transport through the GPEs.[69] Obtained results are depicted in Figure 6, where negative and positive potentials represent Zn-metal stripping and plating, respectively. At a low current density of 50 μA cm^{-2}, all the samples display a reversible Zn-metal plating and stripping behavior, including the glass microfiber separator soaked in 2 M $ZnSO_4$ H_2O. Voltage fluctuations are observed as current density increases, suggesting the growth of a resistive solid electrolyte interphase (SEI) onto the surface of the Zn metal.[70] The glass microfiber separator shows a sudden voltage drop identified as an internal short-circuit with dendrite penetration just after setting the current at 200 μA cm^{-2} (42 h test). This premature short-circuit originates from the inhomogeneous ion transport between Zn surfaces facilitated by the micrometer-sized pores of the separator.[69] On the contrary (magnified view in Figure S6a), the non-cross-linked LS-Chi 30−70 sample provides a nearly square wave shape even at a high current densities of 500 μA cm^{-2} (>100 h test), indicating the occurrence of homogeneous metal ion electrodeposition with reversible Zn/Zn^{2+} redox reactions also at elevated current densities.[20,69]

We conducted a symmetric cycling test under more severe conditions for the LS30Chi70 GPE and observed no short-circuit for areal current densities as high as 5000 μA cm^{-2} (Figure 7a), solving the anode reversibility and stability issues observed in conventional ZIBs. This long-term stability and process reversibility is also confirmed by the high Coulombic efficiency values of above 99.8% for the majority of the compositions studied (Figure S7). More precisely, Coulombic efficiencies approaching 99.5% are observed when the areal current density is below 300 μA cm^{-2}, which is above the values of 99.6% obtained by cyclohexanedodecol-modified $ZnSO_4$ electrolytes[71] or the 99.3% showed by the $Zn(ClO_4)_2$ electrolyte.[72] We ascribe this performance to the reversible Zn^{2+} insertion/extraction originating from the good electrolyte uptake and the ionic conductivity of lignin-GPEs, together with their mechanically adaptative performance (ductility), adhesive properties given by the phenolic hydroxyls,[30] and resistance against dendrite growth (relatively high Young's modulus values). In addition, we also observed that the GPEs having lower lignin fractions present a region of large polarization during the initial three to six stripping/plating cycles for each

https://doi.org/10.1021/acssuschemeng.2c05835
ACS Sustainable Chem. Eng. 2023, 11, 2283−2294

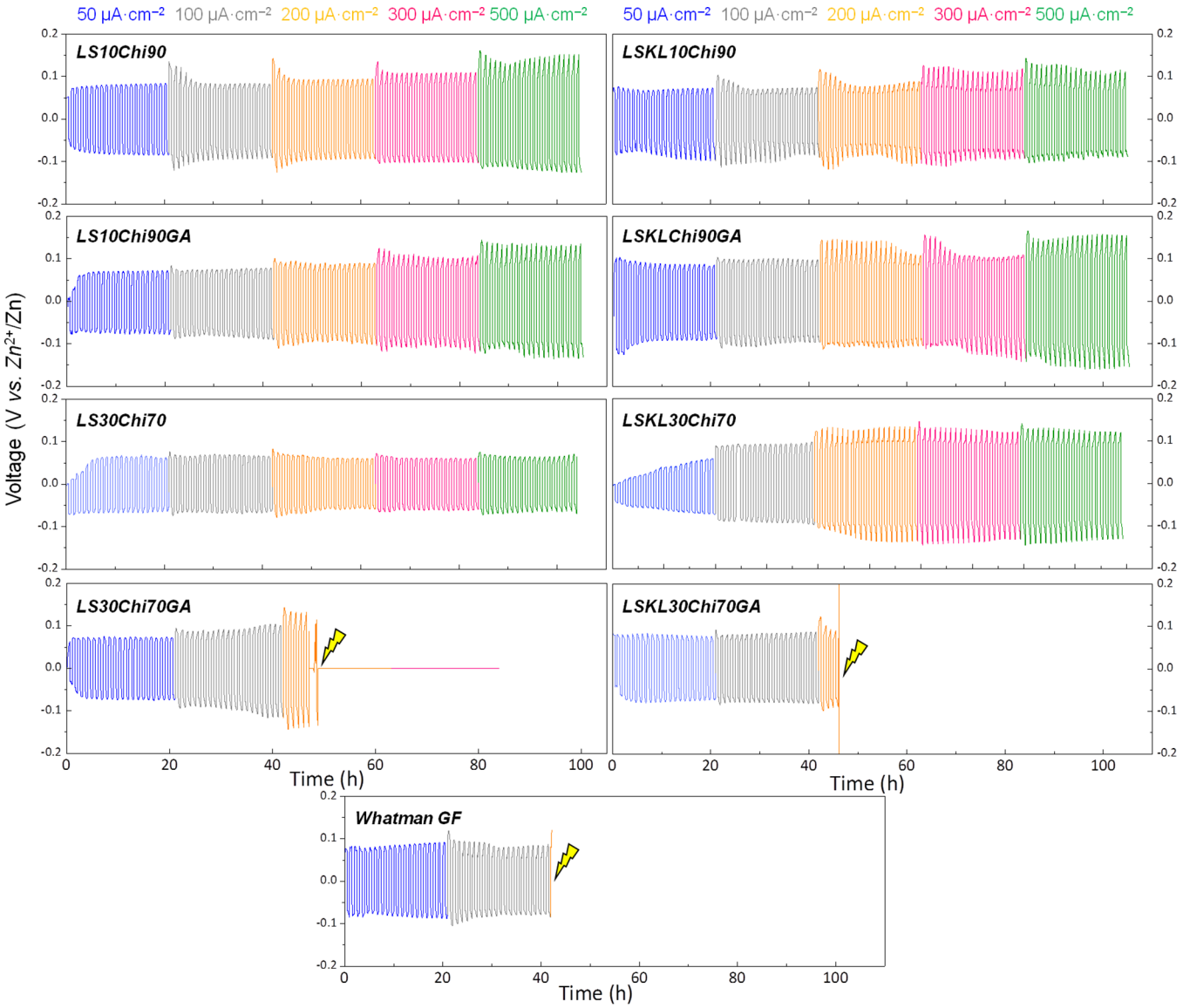

Figure 6. Room-temperature voltage (vertical axis) vs time (horizontal axis) curves for symmetric Zn/Zn cells for Zn plating/stripping at different current densities for lignosulfonate and lignosulfonate/kraft lignin GPEs. Details on the composition of each GPE together with the sample code are provided for each composition. Colors from blue to green represent current densities from ±50 to 500 μA cm^{-2}, while the lightning indicates the occurrence of short-circuit. The curves corresponding to the glass microfiber soaked into 2 M $ZnSO_4$ H_2O are shown for comparison.

current density before reaching a steady-state polarization shape, suggesting a poorer initial interfacial contact (Figure S8).[73]

The extent of overpotential is also a relevant parameter because it indicates the charge transport characteristic, an essential requisite to avoid dendrite formation.[74] Despite the lower ionic conductivity of lignin GPEs over the glass microfiber separator soaked in 2 M $ZnSO_4$ H_2O, comparable overpotential values of ∼160 mV are observed at of 50 μA cm^{-2} for the majority of the samples. It may be concluded thus that the faster Zn^{2+} transport in the glass separator is offset by a smoother and more homogeneous Zn plating/stripping provided by the GPEs, which enables a stable SEI layer.[75] Moreover, notable overpotential differences are observed after 100 h (500 μA cm^{-2}; see Figure S6b), with values ranging from 130 to 318 mV. Overall, glutaraldehyde cross-linking and the substitution of LS by KL seem to increase the overpotential. We ascribe this behavior to the formation of a heterogeneous solid electrolyte interphase on the Zn anode surface.[74] In any case, it is important to note that the low overpotential obtained by the LS,Chi 30/70 GPE enables a high voltage efficiency of the battery, delaying undesired decomposition reactions that may yield to a premature cell failure or inefficient charge/discharge.[74] It is worthy to note that the observed overpotential value for LS30Chi70 GPE is similar to that shown by a cellulose−agarose GPE recently developed by our group, which offers a lifespan extending over 8500 h (one year cycling) in a symmetric Zn|Zn configuration.[23] In fact, we postulate that developed lignin-based GPEs suppress the presence of free water as opposed to conventional membrane/aqueous electrolyte systems, shielding Zn surfaces from the free water-induced Zn corrosion and thus enabling long-term cycling.[32] Noting this composition presents the lower Young's modulus (55 ± 4 MPa), it can be concluded that achieving a good interfacial compatibility and intimate contact of the GPEs with the metallic Zn (also promoted by the hydroxyl and ether

https://doi.org/10.1021/acssuschemeng.2c05835
ACS Sustainable Chem. Eng. 2023, 11, 2283−2294

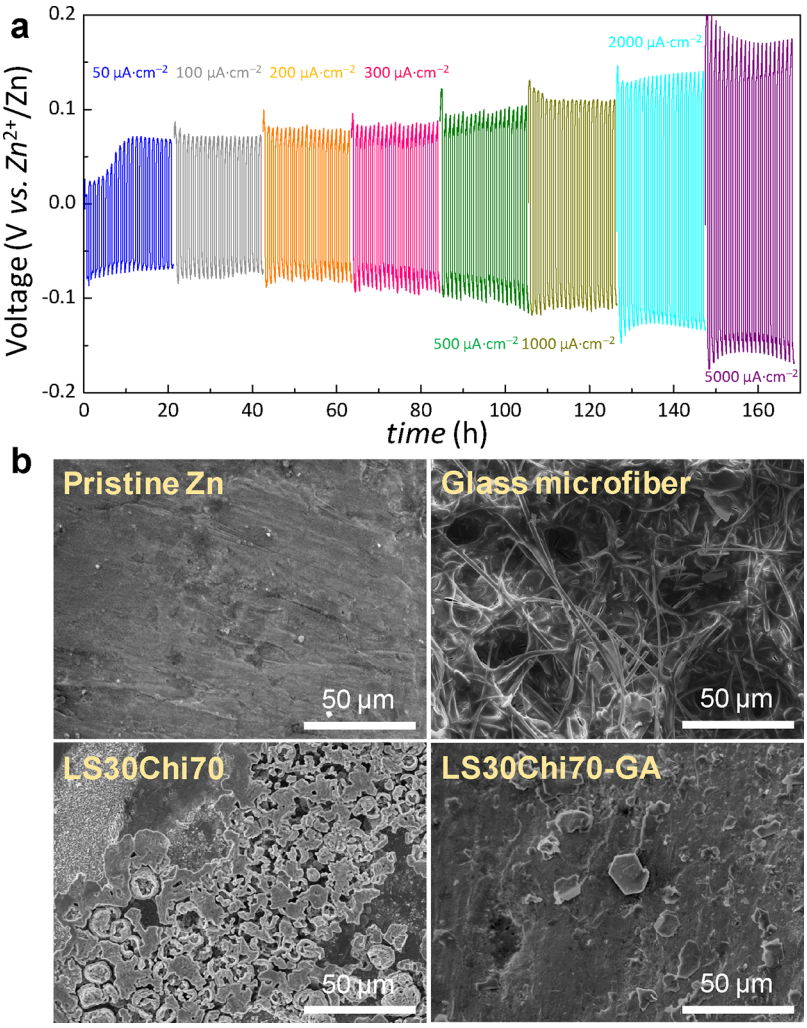

Figure 7. (a) Room-temperature voltage (vertical axis) vs time (horizontal axis) curves for symmetric Zn/Zn cells for the LS30Chi70 GPE at high areal current densities. (b) Post-mortem SEM images of the Zn surfaces after cycling in symmetric Zn/Zn cells using a glass microfiber separator soaked into 2 M $ZnSO_4$ H_2O together with those corresponding to the LS30Chi70 and LS30Chi70 GPEs. The SEM image corresponding to the pristine Zn foil is shown for comparison.

groups in lignin) definitively contribute to reduce the overpotential. In fact, post-mortem SEM and XRD analyses of cycled Zn surfaces in Figure 7b and Figure S9, respectively, prove that the smooth and homogeneous electrodeposition feature of the LS30Chi70 and LS30Chi70GA GPEs is translated into a flat and dendrite-free zinc structure (JCPDS: 36-1451 of metallic zinc). This morphology contrasts with the microscale high-surface area needle-like Zn deposits observed when the symmetric cells separated by a glass microfiber soaked into 2 M $ZnSO_4$ H_2O (short-circuit at 100 μA cm^{-2}). The more abundant deposits observed for the LS30Chi70 GPE over the LS30Chi70GA one may originate from the notably larger current densities, triggering short-circuit (5000 vs 200 μA cm^{-2}).

Considering the functional properties and their renewable/biodegradable nature, we envisage the following potential applications for fabricated lignin-containing GPEs. First, the flexible character of developed GPEs and, in particular, of the samples containing lignosulfonate, is attractive to implement solid-state ZIBs for flexible and wearable electronic devices, where batteries could operate under repeated stretching and bending conditions.[76] Given the versatility of the gelation (physical or chemical), the large ionic conductivities, and mechanical resistance achieved, we foresee a bright future of biopolymer-electrolytes into higher-energy density zinc-ion chemistry batteries. For example, further efforts are needed to incorporate lignin GPEs in secondary zinc-air batteries[77] or in ZIBs comprising metal−organic framework (MOF) cathodes.[78] When lignin−chitosan GPEs are paired with organic cathode materials, fully renewable ZIBs could be obtained, avoiding the use of scarce and toxic critical raw materials that are causing serious resource depletion and supply chain bottleneck issues.[79] Additionally, the biodegradable character of electrolyte constituents makes these GPEs susceptible to degrade under composting conditions, opening new opportunities to fabricate transient rechargeable batteries that are rapidly degraded into harmless by-products (once the adequate trigger is activated) after a period of stable operation.[23] Thereby, lignin−chitosan GPEs have the potential to lessen the inherent environmental impact of conventional LIBs requiring non-biodegradable and harmful materials.

CONCLUSIONS

The production of battery electrolytes adhering to circular economy principles requires a cautious balance between the

https://doi.org/10.1021/acssuschemeng.2c05835
ACS Sustainable Chem. Eng. 2023, 11, 2283−2294

frequently opposing material circularity, safety, cost, and electrochemical performance. On this basis, here, we report the design of a gel polymer electrolyte based on renewable materials suitable for zinc-ion battery chemistries. The easily scalable fabrication approach yields mechanically flexible free-standing ~250 μm thick hydrogels and relies on commercially available lignin and chitosan. The predominantly amorphous structure of the gel polymer electrolyte enhances ion diffusivity, while the available hydroxyl, carboxylic acid, and sulfonate groups coordinate Zn^{2+} to facilitate zinc salt dissociation and render the material with competitive ionic conductivities in the range of 3.8 to 18.6 mS cm^{-1}. The observed wide electrochemical stability window up to +2.2 V vs Zn^{2+}/Zn enables lignin−chitosan GPEs to be used in high-voltage cathode configurations. The synthesized GPEs offer a stable Zn electrodeposition with a nearly square wave-shaped Zn-metal stripping/plating at currents as high as 5000 μA cm^{-2}. This stability represents a clear merit over conventional glass microfiber separator−liquid electrolytes that short-circuit after solely 100 μA cm^{-2} with a notable deviation from the square wave shape. Post-mortem analyses prove that the smooth and homogeneous Zn electrodeposition feature of lignin GPE is translated into a flat and dendrite-free structure. Such improvement is ascribed to the combination of mechanically soft-ductile character of the GPE together with the interplay of free hydroxyl groups and charged sulfonate ions interacting with Zn surfaces that promote an intimate contact with the metallic anode. Overall, our results prove the utility of two major industrial side-streams and waste as resources for the battery electrolyte field, achieving a good electrochemical performance. Consequently, this work paves the way for the implementation of circular material approaches for environmentally sustainable batteries beyond LIBs.

■ ASSOCIATED CONTENT

Data Availability Statement

All the data used to support the findings of this study are included within the article.

Supporting Information

The Supporting Information is available free of charge at https://pubs.acs.org/doi/10.1021/acssuschemeng.2c05835.

Optical photographs, XRD patterns, Nyquist plots, Zn/Zn symmetric tests, and post-mortem XRD analyses of Kraft lignin- and lignosulfonate−chitosan gel polymer electrolytes; tables summarizing sample composition, mechanical parameters, and ionic conductivity quantification (PDF)

■ AUTHOR INFORMATION

Corresponding Authors

Mika H. Sipponen − *Department of Materials and Environmental Chemistry, Stockholm University, SE-106 91 Stockholm, Sweden*; Email: mika.sipponen@mmk.su.se

Erlantz Lizundia − *Life Cycle Thinking Group, Department of Graphic Design and Engineering Projects, Faculty of Engineering in Bilbao, University of the Basque Country (UPV/EHU), 48013 Bilbao, Spain; Basque Center for Materials, Applications and Nanostructures, BCMaterials, 48940 Leioa, Spain;* orcid.org/0000-0003-4013-2721; Email: erlantz.liizundia@ehu.eus

Authors

Naroa Almenara − *Department of Materials and Environmental Chemistry, Stockholm University, SE-106 91 Stockholm, Sweden*

Robin Gueret − *Department of Materials and Environmental Chemistry, Stockholm University, SE-106 91 Stockholm, Sweden*

Alberto J. Huertas-Alonso − *Department of Materials and Environmental Chemistry, Stockholm University, SE-106 91 Stockholm, Sweden;* orcid.org/0000-0002-5632-1802

Unnimaya Thalakkale Veettil − *Department of Materials and Environmental Chemistry, Stockholm University, SE-106 91 Stockholm, Sweden*

Complete contact information is available at: https://pubs.acs.org/10.1021/acssuschemeng.2c05835

Author Contributions

The manuscript was written through contributions of all authors. All authors have given approval to the final version of the manuscript.

Notes

The authors declare the following competing financial interest(s): MHS is a co-owner of Lignoflow Technologies AB, a startup company that owns IPR related to the production of mixed lignin micellar dispersions similar to KL+LS used in the present work.

■ ACKNOWLEDGMENTS

Financial support from the Global Training program of the Basque Government and the "2021 Euskampus Missions 1.0. Programme" granted by Euskampus Fundazioa are acknowledged. The authors are thankful for funds from the University of the Basque Country (Convocatoria de ayudas a grupos de investigacion GIU21/010). Technical and human support provided by SGIker (UPV/EHU, MICINN, GV/EJ, EGEF, and ESF) is gratefully acknowledged. M.H.S. and A.J.H.-A. acknowledge the Swedish Foundation for Strategic Research (SSF) (grant number FFL21-0006) and the Carl Trygger Foundation (grant number CTS 21:1404) for financial support.

■ REFERENCES

(1) Porzio, J.; Scown, C. D. Life-Cycle Assessment Considerations for Batteries and Battery Materials. *Adv. Energy Mater.* **2021**, *11*, 2100771.

(2) Polverini, D. Regulating the Circular Economy within the Ecodesign Directive: Progress so Far, Methodological Challenges and Outlook. *Sustain. Prod. Consum.* **2021**, *27*, 1113−1123.

(3) Mittal, N.; Ojanguren, A.; Niederberger, M.; Lizundia, E. Degradation Behavior, Biocompatibility, Electrochemical Performance, and Circularity Potential of Transient Batteries. *Adv. Sci.* **2021**, *8*, 2004814.

(4) Lebreton, L. C. M.; van der Zwet, J.; Damsteeg, J.-W.; Slat, B.; Andrady, A.; Reisser, J. River Plastic Emissions to the World's Oceans. *Nat. Commun.* **2017**, *8*, 15611.

(5) Cotterman, K. A.; Kendall, A. D.; Basso, B.; Hyndman, D. W. Groundwater Depletion and Climate Change: Future Prospects of Crop Production in the Central High Plains Aquifer. *Clim. Change* **2018**, *146*, 187−200.

(6) York, R.; Bell, S. E. Energy Transitions or Additions?: Why a Transition from Fossil Fuels Requires More than the Growth of Renewable Energy. *Energy Res. Soc. Sci.* **2019**, *51*, 40−43.

(7) Chen, H.; Cong, T. N.; Yang, W.; Tan, C.; Li, Y.; Ding, Y. Progress in Electrical Energy Storage System: A Critical Review. *Prog. Nat. Sci.* **2009**, *19*, 291−312.
(8) Nitta, N.; Wu, F.; Lee, J. T.; Yushin, G. Li-Ion Battery Materials: Present and Future. *Mater. Today* **2015**, *18*, 252−264.
(9) Titirici, M.-M. Sustainable Batteries—Quo Vadis? *Adv. Energy Mater.* **2021**, *11*, 2003700.
(10) Rey, I.; Vallejo, C.; Santiago, G.; Iturrondobeitia, M.; Lizundia, E. Environmental Impacts of Graphite Recycling from Spent Lithium-Ion Batteries Based on Life Cycle Assessment. *ACS Sustainable Chem. Eng.* **2021**, *9*, 14488−14501.
(11) Blanc, L. E.; Kundu, D.; Nazar, L. F. Scientific Challenges for the Implementation of Zn-Ion Batteries. *Joule* **2020**, *4*, 771−799.
(12) Rajput, N. N.; Seguin, T. J.; Wood, B. M.; Qu, X.; Persson, K. A. Elucidating Solvation Structures for Rational Design of Multivalent Electrolytes—A Review. *Top. Curr. Chem.* **2018**, *376*, 19.
(13) Iturrondobeitia, M.; Akizu-Gardoki, O.; Amondarain, O.; Minguez, R.; Lizundia, E. Environmental Impacts of Aqueous Zinc Ion Batteries Based on Life Cycle Assessment. *Adv. Sustain. Syst.* **2022**, *6*, 2100308.
(14) Posada, J. O. G.; Rennie, A. J. R.; Villar, S. P.; Martins, V. L.; Marinaccio, J.; Barnes, A.; Glover, C. F.; Worsley, D. A.; Hall, P. J. Aqueous Batteries as Grid Scale Energy Storage Solutions. *Renewable Sustainable Energy Rev.* **2017**, *68*, 1174−1182.
(15) Wang, Y.; Zhai, F.; Zhou, Q.; Lv, Z.; Jian, L.; Han, P.; Zhou, X.; Cui, G. Functional Applications of Polymer Electrolytes in High-Energy-Density Lithium Batteries. *Macromol. Chem. Phys.* **2022**, *223*, 2100410.
(16) Liu, W.; Jiang, Y.; Wang, N.; Fu, W. Recent Progress in Flame Retardant Technology of Battery: A Review. *Resour. Chem. Mater.* **2023**, *2*, 80−99.
(17) Ferrari, S.; Falco, M.; Muñoz-García, A. B.; Bonomo, M.; Brutti, S.; Pavone, M.; Gerbaldi, C. Solid-State Post Li Metal Ion Batteries: A Sustainable Forthcoming Reality? *Adv. Energy Mater.* **2021**, *11*, 2100785.
(18) Mittal, N.; Tien, S.; Lizundia, E.; Niederberger, M. Hierarchical Nanocellulose-Based Gel Polymer Electrolytes for Stable Na Electrodeposition in Sodium Ion Batteries. *Small* **2022**, *18*, 2107183.
(19) Zhou, D.; Shanmukaraj, D.; Tkacheva, A.; Armand, M.; Wang, G. Polymer Electrolytes for Lithium-Based Batteries: Advances and Prospects. *Chem* **2019**, *5*, 2326−2352.
(20) Qiu, H.; Hu, R.; Du, X.; Chen, Z.; Zhao, J.; Lu, G.; Jiang, M.; Kong, Q.; Yan, Y.; Du, J.; Zhou, X.; Cui, G. Eutectic Crystallization Activates Solid-State Zinc-Ion Conduction. *Angew. Chem., Int. Ed.* **2022**, *61*, No. e202113086.
(21) Wang, W.; Li, Z.; Huang, H.; Li, W.; Wang, J. Facile Design of Novel Nanocellulose-Based Gel Polymer Electrolyte for Lithium-Ion Batteries Application. *Chem. Eng. J.* **2022**, *445*, 136568.
(22) Ge, X.; Zhang, W.; Song, F.; Xie, B.; Li, J.; Wang, J.; Wang, X.; Zhao, J.; Cui, G. Single-Ion-Functionalized Nanocellulose Membranes Enable Lean-Electrolyte and Deeply Cycled Aqueous Zinc-Metal Batteries. *Adv. Funct. Mater.* **2022**, *32*, 2200429.
(23) Mittal, N.; Ojanguren, A.; Kundu, D.; Lizundia, E.; Niederberger, M. Bottom-Up Design of a Green and Transient Zinc-Ion Battery with Ultralong Lifespan. *Small* **2022**, 2206249.
(24) Wu, M.; Zhang, Y.; Xu, L.; Yang, C.; Hong, M.; Cui, M.; Clifford, B. C.; He, S.; Jing, S.; Yao, Y.; Hu, L. A Sustainable Chitosan-Zinc Electrolyte for High-Rate Zinc-Metal Batteries. *Matter* **2022**, *5*, 3402−3416.
(25) Ecologic Institute2018. *Top emerging bio-based products, their properties and industrial applications*; Ecologic Institute: Berlin.
(26) Dessbesell, L.; Paleologou, M.; Leitch, M.; Pulkki, R.; Xu, C. (. C.). Global Lignin Supply Overview and Kraft Lignin Potential as an Alternative for Petroleum-Based Polymers. *Renewable Sustainable Energy Rev.* **2020**, *123*, 109768.
(27) Lizundia, E.; Sipponen, M. H.; Greca, L. G.; Balakshin, M.; Tardy, B. L.; Rojas, O. J.; Publia, D. Multifunctional Lignin-Based Nanocomposites and Nanohybrids. *Green Chem.* **2021**, *23*, 6698−6760.
(28) Ragauskas, A. J.; Beckham, G. T.; Biddy, M. J.; Chandra, R.; Chen, F.; Davis, M. F.; Davison, B. H.; Dixon, R. A.; Gilna, P.; Keller, M.; Langan, P.; Naskar, A. K.; Saddler, J. N.; Tschaplinski, T. J.; Tuskan, G. A.; Wyman, C. E. Lignin Valorization: Improving Lignin Processing in the Biorefinery. *Science* **2014**, *344*, 1246843.
(29) Li, Q.; Cao, D.; Naik, M. T.; Pu, Y.; Sun, X.; Luan, P.; Ragauskas, A. J.; Ji, T.; Zhao, Y.; Chen, F.; Zheng, Y.; Zhu, H. Molecular Engineering of Biorefining Lignin Waste for Solid-State Electrolyte. *ACS Sustainable Chem. Eng.* **2022**, *10*, 8704−8714.
(30) Gendron, J.; Stambouli, I.; Bruel, C.; Boumghar, Y.; Montplaisir, D. Characterization of Different Types of Lignin and Their Potential Use in Green Adhesives. *Ind. Crops Prod.* **2022**, *182*, 114893.
(31) Shabanov, N. S.; Rabadanov, K. S.; Gafurov, M. M.; Isaev, A. B.; Sobola, D. S.; Suleimanov, S. I.; Amirov, A. M.; Asvarov, A. S. Lignin-Based Gel Polymer Electrolyte for Cationic Conductivity. *Polymer* **2021**, *13*, 2306.
(32) Zhao, Z.; Zhao, J.; Hu, Z.; Li, J.; Li, J.; Zhang, Y.; Wang, C.; Cui, G. Long-Life and Deeply Rechargeable Aqueous Zn Anodes Enabled by a Multifunctional Brightener-Inspired Interphase. *Energy Environ. Sci.* **2019**, *12*, 1938−1949.
(33) Pylypchuk, I.; Sipponen, M. H. Organic Solvent-Free Production of Colloidally Stable Spherical Lignin Nanoparticles at High Mass Concentrations. *Green Chem.* **2022**, *24*, 8705−8715.
(34) Rincon-Iglesias, M.; Lizundia, E.; Lanceros-Mendez, S. Water-Soluble Cellulose Derivatives as Suitable Matrices for Multifunctional Materials. *Biomacromolecules* **2019**, *20*, 2786−2795.
(35) Zhang, H.; Armand, M. History of Solid Polymer Electrolyte-Based Solid-State Lithium Metal Batteries: A Personal Account. *Isr. J. Chem.* **2021**, *61*, 94−100.
(36) Bai, L.; Liu, L.; Esquivel, M.; Tardy, B. L.; Huan, S.; Niu, X.; Liu, S.; Yang, G.; Fan, Y.; Rojas, O. J. Nanochitin: Chemistry, Structure, Assembly, and Applications. *Chem. Rev.* **2022**, *122*, 11604−11674 DOI: Nanochitin: Chemistry, Structure, Assembly, and Applications.
(37) Hao, G.; Hu, Y.; Shi, L.; Chen, J.; Cui, A.; Weng, W.; Osako, K. Physicochemical Characteristics of Chitosan from Swimming Crab (Portunus Trituberculatus) Shells Prepared by Subcritical Water Pretreatment. *Sci. Rep.* **2021**, *11*, 1646.
(38) Juikar, S. J.; Vigneshwaran, N. Extraction of Nanolignin from Coconut Fibers by Controlled Microbial Hydrolysis. *Ind. Crops Prod.* **2017**, *109*, 420−425.
(39) Lee, S.; Nam, S.; Choi, Y.; Kim, M.; Koo, J.; Chae, B.-J.; Kang, W.-S.; Cho, H.-J. Fabrication and Characterizations of Hot-Melt Extruded Nanocomposites Based on Zinc Sulfate Monohydrate and Soluplus. *Appl. Sci.* **2017**, *7*, 902.
(40) Lee, H.; Yanilmaz, M.; Toprakci, O.; Fu, K.; Zhang, X. A Review of Recent Developments in Membrane Separators for Rechargeable Lithium-Ion Batteries. *Energy Environ. Sci.* **2014**, *7*, 3857−3886.
(41) Faix, O.*Fourier Transform Infrared Spectroscopy BT - Methods in Lignin Chemistry*; Lin, S. Y., Dence, C. W., Eds.; Springer Berlin Heidelberg: Berlin, Heidelberg, 1992; 233−241.
(42) Villar-Chavero, M. M.; Domínguez, J. C.; Alonso, M. V.; Oliet, M.; Rodriguez, F. Thermal and Kinetics of the Degradation of Chitosan with Different Deacetylation Degrees under Oxidizing Atmosphere. *Thermochim. Acta* **2018**, *670*, 18−26.
(43) Wu, N.; Ding, C.; Yang, R. Effects of Zinc and Nickel Salts in Intumescent Flame-Retardant Polypropylene. *Polym. Degrad. Stab.* **2010**, *95*, 2589−2595.
(44) Ojanguren, A.; Mittal, N.; Lizundia, E.; Niederberger, M. Stable Na Electrodeposition Enabled by Agarose-Based Water-Soluble Sodium Ion Battery Separators. *ACS Appl. Mater. Interfaces* **2021**, *13*, 21250−21260.
(45) Alongi, J.; Han, Z.; Bourbigot, S. Intumescence: Tradition versus Novelty. A Comprehensive Review. *Prog. Polym. Sci.* **2015**, *51*, 28−73.

https://doi.org/10.1021/acssuschemeng.2c05835
ACS Sustainable Chem. Eng. 2023, 11, 2283−2294

(46) Liu, Z.; Jiang, Y.; Hu, Q.; Guo, S.; Yu, L.; Li, Q.; Liu, Q.; Hu, X. Safer Lithium-Ion Batteries from the Separator Aspect: Development and Future Perspectives. *Energy Environ. Mater.* **2021**, *4*, 336−362.
(47) Zhang, S. S. A Review on the Separators of Liquid Electrolyte Li-Ion Batteries. *J. Power Sources* **2007**, *164*, 351−364.
(48) Zhou, H.; Gu, J.; Zhang, W.; Hu, C.; Lin, X. Rational Design of Cellulose Nanofibrils Separator for Sodium-Ion Batteries. *Molecules* **2021**, *26*, 5539.
(49) Crouvisier-Urion, K.; Bodart, P. R.; Winckler, P.; Raya, J.; Gougeon, R. D.; Cayot, P.; Domenek, S.; Debeaufort, F.; Karbowiak, T. Biobased Composite Films from Chitosan and Lignin: Antioxidant Activity Related to Structure and Moisture. *ACS Sustainable Chem. Eng.* **2016**, *4*, 6371−6381.
(50) Rosova, E.; Smirnova, N.; Dresvyanina, E.; Smirnova, V.; Vlasova, E.; Ivan'kova, E.; Sokolova, M.; Maslennikova, T.; Malafeev, K.; Kolbe, K.; Kanerva, M.; Yudin, V. Biocomposite Materials Based on Chitosan and Lignin: Preparation and Characterization. *Cosmetics* **2021**, *8*, 24.
(51) Izaguirre, N.; Gordobil, O.; Robles, E.; Labidi, J. Enhancement of UV Absorbance and Mechanical Properties of Chitosan Films by the Incorporation of Solvolytically Fractionated Lignins. *Int. J. Biol. Macromol.* **2020**, *155*, 447−455.
(52) Liu, H.; Cheng, X.-B.; Huang, J.-Q.; Yuan, H.; Lu, Y.; Yan, C.; Zhu, G.-L.; Xu, R.; Zhao, C.-Z.; Hou, L.-P.; He, C.; Kaskel, S.; Zhang, Q. Controlling Dendrite Growth in Solid-State Electrolytes. *ACS Energy Lett.* **2020**, *5*, 833−843.
(53) Huang, Q.; Song, J.; Gao, Y.; Wang, D.; Liu, S.; Peng, S.; Usher, C.; Goliaszewski, A.; Wang, D. Supremely Elastic Gel Polymer Electrolyte Enables a Reliable Electrode Structure for Silicon-Based Anodes. *Nat. Commun.* **2019**, *10*, 5586.
(54) Farzin, S.; Johnson, T. J.; Chatterjee, S.; Zamani, E.; Dishari, S. K. Ionomers From Kraft Lignin for Renewable Energy Applications. *Front. Chem.* **2020**, *8*, 690.
(55) Gordobil, O.; Herrera, R.; Poohphajai, F.; Sandak, J.; Sandak, A. Impact of Drying Process on Kraft Lignin: Lignin-Water Interaction Mechanism Study by 2D NIR Correlation Spectroscopy. *J. Mater. Res. Technol.* **2021**, *12*, 159−169.
(56) Leskinen, T.; Witos, J.; Valle Delgado, J. J.; Lintinen, K. S.; Kostiainen, M. A.; Wiedmer, S. K.; Österberg, M.; Mattinen, M.-L. Adsorption of Proteins on Colloidal Lignin Particles for Advanced Biomaterials. *Biomacromolecules* **2017**, *18*, 2767−2776.
(57) Baloch, M.; Alberro, M.; Labidi, J. Electrochemical Activity of Lignin Based Composite Membranes. *Polymer* **2021**, *13*, 643.
(58) Ye, J.; Cheng, Y.; Sun, L.; Ding, M.; Wu, C.; Yuan, D.; Zhao, X.; Xiang, C.; Jia, C. A Green SPEEK/Lignin Composite Membrane with High Ion Selectivity for Vanadium Redox Flow Battery. *J. Memb. Sci.* **2019**, *572*, 110−118.
(59) Gong, S.-D.; Huang, Y.; Cao, H.-J.; Lin, Y.-H.; Li, Y.; Tang, S.-H.; Wang, M.-S.; Li, X. A Green and Environment-Friendly Gel Polymer Electrolyte with Higher Performances Based on the Natural Matrix of Lignin. *J. Power Sources* **2016**, *307*, 624−633.
(60) Dueramae, I.; Okhawilai, M.; Kasemsiri, P.; Uyama, H. High Electrochemical and Mechanical Performance of Zinc Conducting-Based Gel Polymer Electrolytes. *Sci. Rep.* **2021**, *11*, 13268.
(61) Zhang, S.; Yu, N.; Zeng, S.; Zhou, S.; Chen, M.; Di, J.; Li, Q. An Adaptive and Stable Bio-Electrolyte for Rechargeable Zn-Ion Batteries. *J. Mater. Chem. A* **2018**, *6*, 12237−12243.
(62) Jia, X.; Yang, Y.; Wang, C.; Zhao, C.; Vijayaraghavan, R.; MacFarlane, D. R.; Forsyth, M.; Wallace, G. G. Biocompatible Ionic Liquid−Biopolymer Electrolyte-Enabled Thin and Compact Magnesium−Air Batteries. *ACS Appl. Mater. Interfaces* **2014**, *6*, 21110−21117.
(63) Liu, B.; Huang, Y.; Cao, H.; Song, A.; Lin, Y.; Wang, M.; Li, X. A High-Performance and Environment-Friendly Gel Polymer Electrolyte for Lithium Ion Battery Based on Composited Lignin Membrane. *J. Solid State Electrochem.* **2018**, *22*, 807−816.
(64) Yuan, D.; Manalastas, W., Jr.; Zhang, L.; Chan, J. J.; Meng, S.; Chen, Y.; Srinivasan, M. Lignin@Nafion Membranes Forming Zn Solid−Electrolyte Interfaces Enhance the Cycle Life for Rechargeable Zinc-Ion Batteries. *ChemSusChem* **2019**, *12*, 4889−4900.
(65) Lu, G.; Zhang, Y.; Zhang, J.; Du, X.; Lv, Z.; Du, J.; Zhao, Z.; Tang, Y.; Zhao, J.; Cui, G. Trade-Offs between Ion-Conducting and Mechanical Properties: The Case of Polyacrylate Electrolytes. *Carbon Energy* **2022**, DOI: 10.1002/cey2.287.
(66) Abbasi, A.; Xu, Y.; Khezri, R.; Etesami, M.; Lin, C.; Kheawhom, S.; Lu, Y. Advances in Characteristics Improvement of Polymeric Membranes/Separators for Zinc-Air Batteries. *Mater. Today Sustain.* **2022**, *18*, 100126.
(67) Ma, L.; Chen, S.; Li, N.; Liu, Z.; Tang, Z.; Zapien, J. A.; Chen, S.; Fan, J.; Zhi, C. Hydrogen-Free and Dendrite-Free All-Solid-State Zn-Ion Batteries. *Adv. Mater.* **2020**, *32*, 1908121.
(68) Wang, S.; Zhang, L.; Wang, A.; Liu, X.; Chen, J.; Wang, Z.; Zeng, Q.; Zhou, H.; Jiang, X.; Zhang, L. Polymer-Laden Composite Lignin-Based Electrolyte Membrane for High-Performance Lithium Batteries. *ACS Sustainable Chem. Eng.* **2018**, *6*, 14460−14469.
(69) Hänsel, C.; Lizundia, E.; Kundu, D. A Single Li-Ion Conductor Based on Cellulose. *ACS Appl. Energy Mater.* **2019**, *2*, 5686−5691.
(70) Xia, S.; Lopez, J.; Liang, C.; Zhang, Z.; Bao, Z.; Cui, Y.; Liu, W. High-Rate and Large-Capacity Lithium Metal Anode Enabled by Volume Conformal and Self-Healable Composite Polymer Electrolyte. *Adv. Sci.* **2019**, *6*, 1802353.
(71) Wu, Z.; Li, M.; Tian, Y.; Chen, H.; Zhang, S.-J.; Sun, C.; Li, C.; Kiefel, M.; Lai, C.; Lin, Z.; Zhang, S. Cyclohexanedodecol-Assisted Interfacial Engineering for Robust and High-Performance Zinc Metal Anode. *Nano-Micro Lett.* **2022**, *14*, 110.
(72) Wang, L.; Zhang, Y.; Hu, H.; Shi, H.-Y.; Song, Y.; Guo, D.; Liu, X.-X.; Sun, X. A $Zn(ClO_4)_2$ Electrolyte Enabling Long-Life Zinc Metal Electrodes for Rechargeable Aqueous Zinc Batteries. *ACS Appl. Mater. Interfaces* **2019**, *11*, 42000−42005.
(73) Chen, N.; Dai, Y.; Xing, Y.; Wang, L.; Guo, C.; Chen, R.; Guo, S.; Wu, F. Biomimetic Ant-Nest Ionogel Electrolyte Boosts the Performance of Dendrite-Free Lithium Batteries. *Energy Environ. Sci.* **2017**, *10*, 1660−1667.
(74) Liu, M.; Cheng, Z.; Qian, K.; Verhallen, T.; Wang, C.; Wagemaker, M. Efficient Li-Metal Plating/Stripping in Carbonate Electrolytes Using a $LiNO_3$-Gel Polymer Electrolyte, Monitored by Operando Neutron Depth Profiling. *Chem. Mater.* **2019**, *31*, 4564−4574.
(75) Jeong, D.; Shim, J.; Shin, H.; Lee, J.-C. Sustainable Lignin-Derived Cross-Linked Graft Polymers as Electrolyte and Binder Materials for Lithium Metal Batteries. *ChemSusChem* **2020**, *13*, 2642−2649.
(76) Xu, W.; Liu, C.; Wu, Q.; Xie, W.; Kim, W.-Y.; Lee, S.-Y.; Gwon, J. A Stretchable Solid-State Zinc Ion Battery Based on a Cellulose Nanofiber−Polyacrylamide Hydrogel Electrolyte and a $Mg_{0.23}V_2O_5 \cdot 1.0H_2O$ Cathode. *J. Mater. Chem. A* **2020**, *8*, 18327−18337.
(77) Frattini, D.; García Gaitán, E.; Bustinza Murguialday, A.; Armand, M.; Ortiz-Vitoriano, N. Essential Data for Industrially Relevant Development of Bifunctional Cathodes and Biopolymer Electrolytes in Solid-State Zinc−Air Secondary Batteries. *Energy Environ. Sci.* **2022**, *15*, 5039−5058.
(78) Zhao, T.; Wu, H.; Wen, X.; Zhang, J.; Tang, H.; Deng, Y.; Liao, S.; Tian, X. Recent Advances in MOFs/MOF Derived Nanomaterials toward High-Efficiency Aqueous Zinc Ion Batteries. *Coord. Chem. Rev.* **2022**, *468*, 214642.
(79) Cui, H.; Ma, L.; Huang, Z.; Chen, Z.; Zhi, C. Organic Materials-Based Cathode for Zinc Ion Battery. *SmartMat* **2022**, *3*, 565−581.